INTERNATIONAL JOURNAL OF HYDROGEN ENERGY 48 (2023) 27892–27906

Available online at www.sciencedirect.com

ScienceDirect

journal homepage: www.elsevier.com/locate/he

Coupling the solvent-based CO_2 capture processes to the metal water-splitting for hydrogen generation in a semi-continuous system

Juan I. del Rio [a,b], *Angel Martin* [a,*], *Maria D. Bermejo* [a]

[a] *BioEcoUva, Bioeconomy Research Institute, PressTech Group, Department of Chemical Engineering and Environmental Technology, Universidad de Valladolid, Prado de La Magdalena S/n, 47011 Valladolid, Spain*
[b] *Grupo Procesos Químicos Industriales, Department of Chemical Engineering, Universidad de Antioquia UdeA, Calle 70 No. 52-21, Medellín 050010, Colombia*

HIGHLIGHTS

- A novel semicontinuos facility was designed for H_2 generation from water-splitting.
- Aqueous NaOH promoted the highest H_2 yield of 85.5%.
- H_2 yield increased in the order Al < Mn < Fe < Zn, using ammonium carbamate as CO2RS.
- Most basic CO2RSs and CO2LSs produce a bigger effect with larger metal-particles.
- H_2 generation with Al and NaOH proceeded in a self-sustaining way at room temperature.

GRAPHICAL ABSTRACT

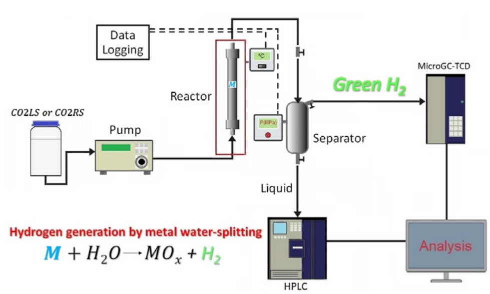

ARTICLE INFO

Article history:
Received 28 February 2023
Received in revised form 31 March 2023
Accepted 2 April 2023
Available online 18 April 2023

Keywords:
Green hydrogen

ABSTRACT

Hydrogen is considered as the future energy vector. Due to scarceness in materials, obtaining hydrogen from common metals and metallic residues is gaining interest. The present work aims at coupling for the first time solvent-based CO_2 capture processes with the hydrogen generation from the metal-water splitting reaction, using common elements such as Al, Zn, Mn and Fe. To do so, a novel semicontinuous facility is developed. In the process, both the CO_2-Rich stream (CO2RS) and CO_2 Capture-Solvent Lean stream (CO2LS) are considered. The production of H_2 increased in the order Al < Mn < Fe < Zn. For pure Al, aqueous NaOH (CO2LS) showed the highest H_2 yield, up to 85.5%, while Al chips (residue) showed outstanding performance. The experimental study showed that small particle

* *Corresponding author.*
E-mail address: mamaan@iq.uva.es (A. Martin).
https://doi.org/10.1016/j.ijhydene.2023.04.021

H_2-economy
CO_2-Economy
Metal-water splitting
Superheated water
Semicontinuous facility

sizes improve the H_2 yield. This technology represents an opportunity for bringing about value-added to CO_2 capture by generating at the same time green hydrogen.

Nomenclature

AC	ammonium carbamate
$C_{CS,f}$	final molar concentration of carbamate
$C_{CS,i}$	initial molar concentration of carbamate
CO2LS	alkaline CO_2 Capture-Solvent Lean stream
CO2RS	alkaline CO_2-Rich stream
lCO2	CO_2 conversion
MB	metallic bed in reactor R-101
MW_{RM}	molecular weight of RM
$n_{H2,MB}$	total moles of hydrogen that can be obtained from the total moles of RMs in MB if the conversion of its corresponding metal-water splitting reaction is 100%
nH2	moles of hydrogen produced
$nH2_{STP}$	moles of hydrogen expressed in STP
$n_{RM,MB}$	moles of RM in MB
PRM	pure reducing metal (commercial reagent) as MB
$P_{s,f}$	final absolute pressure (P3) inside the unit S-101
R	ideal gas constant (83.14472 L*mbar*K^{-1}*mol^{-1})
$R_{H2,RM}$	ratio of moles of hydrogen that can be produced per mole of RM (see Table 1S)
RM	reducing metal (element)
SB	sodium bicarbonate
STP	standard temperature and pressure (1 atm and 0 °C)
STT	steady temperature time (hours)
$T_{s,f}$	final temperature (T3)
Vn_{STP}	molar volume of hydrogen at STP
$V_{s,f}$	final overhead (gas) volume inside unit S-101
Vs,f_{STP}	final overhead (gas) volume at STP
$V_{s,l}$	final volume of liquid collected in S-101
$V_{s,t}$	total volume of S-101
W_{MB}	initial weight of MB
xH2	fractional molar composition of hydrogen, measured by MicroGC-TCD
X_{RM}	mass composition (wt%) of RM in the MB
YH2	hydrogen yield
φH2	hydrogen generation rate at STP

Introduction

In recent times, the increasing of goods and services is leading to a rapid diversification of the energy basket in many countries [1]. However, about 50% of the energy production by 2050 will still come from fossil fuels [2]. To meet the CO_2 global targets, the IEA (International Energy Agency) emphasizes the importance of CCUS (Carbon Capture, Utilization and Storage) technologies, capable of providing up to 20% of the emissions cuts needed by 2050 [3]. In this matter, the solvent based post-combustion CO_2 capture processes, with subsequent geo-sequestration, occupy an important share in the efforts for CO_2 emissions abatement. One of the most developed technologies consists of the absorption of CO_2 with aqueous solutions of amines (generally known as CO_2 Capture-Solvent Lean stream, CO2LS, for any basic dissolution) in absorber/stripper columns, yielding a CO_2-Rich stream (CO2RS) containing anion species in equilibria (e.g., bicarbonate, carbonate and carbamate) [4,5]. For its part, carbonate/bicarbonate solvent-based CO_2 capture systems have positive features such as low cost, low toxicity, ease of regeneration, slow corrosiveness, low degradation, high stability, and CO_2 absorption capacity [6]. Over 700 plants worldwide have implemented the potassium carbonate solution for CO_2 and hydrogen sulphide removal [7]. In the same way, NaOH is an ideal absorbent for carbon capture because its low cost, low toxicity, high accessibility [6], and, for instance, it has been industrially implemented in the SkyMine® process (Capitol Aggregates' San Antonio cement plant in Texas), while yielding marketable by-products, such as baking soda, hydrochloric acid, and bleach [8]. Nevertheless, storing CO_2 is not sufficient in the growing demand for products and services. On the contrary, CO_2 can acquire added-value when incorporated to the transformation processes into useful products, such as fuels or chemicals [9].

In parallel, the hydrogen economy, driven by renewable sources, supposes a breakthrough in future's sustainability [10], and a priority for the EU's post-COVID-19 economic recovery [11,12]. Pure hydrogen is a promising fuel because of its high calorific value (120–143 MJ/kg) compared to coal (14–29.6 MJ/kg) [13,14]. Currently, it is almost entirely supplied from natural gas (converted by steam methane reforming), but it can be obtained by a number of processes such as water electrolysis, gasification of coal and biomass, biological processes, water splitting by high temperature heat, and photocatalytic and electrocatalytic hydrogen evolution reaction (HER) using metal-organic frameworks (MOFs) and bimetallic phosphides (BMPs) [15–19]. The production from fossil sources (grey-hydrogen) has a significant carbon emission (around 830 million tons of carbon dioxide per year) [20], which has to be cut in about 30% the methane leakage associated to the production and supply chains, according to COP 26 [21], making necessary to change to low- or zero-carbon hydrogen production [22]. In this context, blue-hydrogen is the cleaner version of grey, where the carbon emissions are captured and geologically stored or reused. Green hydrogen is the cleanest version; it is generated by renewable energy sources (i.e., water electrolysis) without producing carbon emissions, using low or zero-carbon electricity [23].

Although only green hydrogen is considered by EU as a target fuel for the future, and blue hydrogen does not comply the IPCEI rules (Important Projects of Common European Interests) [24], blue hydrogen may have an important place as an intermediate solution in the coming decades, especially if the CO_2 capture rate can be kept to 99% [25]. The main problem with blue hydrogen is that, its reduction impact on the greenhouse effect has not been fully proven, since the effective reduction of CO_2 emissions is only 9–12% less than grey, and the footprint of greenhouse gases can be more than 20% higher than burning natural gas or coal, and 60% higher than burning diesel, according to recent life cycle analysis proposed by Howarth et al. [26]. Even so, blue hydrogen has competitive advantages, and its achievement cannot be ruled out in the medium term, since it will be cheaper than green hydrogen, especially by 2030 [27], and with greater potential for industrial scaling [28]. In consequence, efforts are addressed toward a cleaner and environmentally sustainable way of production of green hydrogen. The electrolysis of water, mainly using alkaline and PEM (proton exchange membrane) electrolyzers, as hydrogen production system is a proven technology in small and large scale [29], but its disadvantages are the high cost of components, use of noble catalysts, low durability, corrosion, among others [30]. In general, electrolysis is still a more expensive method (~$6/kg with wind as energy source) compared to traditional steam reforming ($2.27/kg) and only applied if high-purity hydrogen is required [20,31,32].

Since the past decade, hydrogen generated from the reaction or corrosion of aluminum/aluminum alloys with water becomes interesting because of its low cost, relatively high hydrogen storage capacity and simplicity of the hydrogen generation system [33]. In spite of the need of further economic assessments to ensure feasibility of aluminum as feedstock, the process is promising in terms of sustainability, owing to the recyclability of aluminum from scrap, using renewable energy [34], as aluminum can be regenerated through a solar thermochemical cycle [35,36], or a two-step thermochemical water splitting using microwage heating under low temperatures from advanced nuclear power plants, where the exhausted/oxidized metals can be recovered by thermal reduction [37]. Recycled scrap aluminum, not suitable for secondary aluminum production, can be consumed for hydrogen generation, making the cost of aluminum-based hydrogen production potentially low [38]. Other aluminum containing waste materials, like capacitors, aluminum cans and packaging, suppose an important feedstock for H_2 generation, because they would not require complicated separation processes, as the non-aluminum parts (plastic, paper, etc) do not have substantial influence on the mechanism of hydrogen production [39]. Besides, the hydrogen mass yield of the aluminum-water splitting of 11.1% is competitive with other renewable sources of hydrogen like steam gasification of biomass (hydrogen yield potential of 7.6–12.6%), and can be obtained under milder reaction temperature, while gasification requires above 700 °C [40].

The hydrogen release rate from aluminum in water without activation is low, only of the order of 5.56e-7 L H_2/sec/g of Al [41]. This is why aluminum has to be properly surface-activated, and many approaches have been studied, like milling and ultrasonic treatment, higher reaction temperatures, preparation of alloys of aluminum by adding other metals, like Ni, Co or Ga [42,43], reducing the size of aluminum particles, use of acids or bases, and inorganic water-soluble salts like KCl and NaCl [44–48].

The activation of aluminum by water and alkaline solutions, mainly aqueous NaOH, has been widely reported [49–52]. The process takes place through reactions 1 and 2 [53]:

$$2Al+6H_2O \rightarrow 2Al(OH)_3+3H_2 \quad (1)$$

$$2Al + 2NaOH + 6H_2O \rightarrow 2NaAl(OH)_4 + 3H_2 \quad (2)$$

This technology has proven to be efficient. Its disadvantages are the corrosive nature of NaOH and its additional cost as raw material. Another alkaline solution like KOH was tasted under flow conditions in an annular reactor, pumped through an annular reactor where it contacts the Al foil wrapped on the surface of the inner rod [54]. A similar efficiency to NaOH was obtained, given its strong base nature, but the formation of a fluffy and sticky dense layer of Al_xOH_y is a disadvantage, as it covered the Al surface, thus preventing the hydrogen generation to proceed continuously, so removal of this layer is a challenge to be solved [33]. For instance, for Manganese (Mn) corrosion (reaction 3) the addition of ammonium salts, like CH_3COONH_4, has been studied to coagulate the $Mn(OH)_2$ passive layer that inhibits the H_2 generation reaction to proceed [55]. When producing hydrogen from iron in water (reaction 4), Michiels et al. [56] demonstrated the benefits of using carbon dioxide (reaction 5), because an unstable carbonate intermediate ($FeCO_3$) is formed in mild hydrothermal condition, which is unstable and hydrates to Fe_3O_4, H_2 and CO_2 (reaction 6), so carbonate ions CO_3^{-2} play a catalytic role. Likewise, Zn (reaction 7) is known for its great potential as redox pair (ZnO/Zn) for solar-driven thermochemical water-splitting based hydrogen generation [57].

$$Mn + H_2O \rightarrow MnO + H_2 \quad (3)$$

$$3Fe+4H_2O \rightarrow Fe_3O_4+4H_2 \quad (4)$$

$$Fe + CO_2+H_2O \rightarrow FeCO_3+H_2 \quad (5)$$

$$3FeCO_3+H_2O \rightarrow Fe_3O_4+H_2+3CO_2 \quad (6)$$

$$Zn + H_2O \rightarrow ZnO + H_2 \quad (7)$$

There is a vast number of studies in batch mode for hydrogen generation, but it is evident from the literature [58] that: *"It is necessary to consider reactor operation in different regimes such as pulse, quasicontinuous, and flowing"*, where only counted works have attempted. Among them, it can be mentioned the work of Hikari et al. [59], who also implemented a semi-continuous system for the generation of high-pressure hydrogen (30 MPa), using waste aluminum with 15% content of metallic Al, under subcritical water, yielding 16.7 g H_2/kg Al. In the work of Takahashi et al. [60], a flow-type equipment was implemented for the continuous reduction of CO_2 dissolved in 0.01 mol/L HCl aqueous solution, at 2.0 MPa through a Fe powder bed, mainly yielding methane, ethylene, ethane and propylene. The use of carbon steel (S–45C) cutting chaffs as the reductant, with Ni powder as hydrogenation catalyst, made possible to generate hydrogen, CO and formic acid. Most recently, Roychowdhury et al. [61] used a $Rh/CeO_2/\gamma\text{-}Al_2O_3$ catalyst in a continuous system for generating hydrogen from both the steam reforming of methanol (SRM) and the thermochemical water splitting (TCWS). The role of rhodium is to effectively cleave the C–C bond of ethanol into hydrogen and promote the reducibility CeO_2 during redox cycles. This combined approach reaches a 67%vol of H_2 from SRM, and a H_2 amount of 48.9 mmol/g_{cat} in four redox cycles from TCWS, but at the cost of high temperature conditions (400-1200 °C) and rhodium and cerium as expensive rare metals.

Despite these reports, the CO_2 Capture-Solvent Lean stream (CO2LS) and CO_2-Rich stream (CO2RS) coming from the solvents-based CO_2 capture processes, have not been proposed nor studied as activators/catalyzers of the metal water-splitting reaction for green hydrogen production in a semicontinuous fashion. On the other hand, many works have published the effect of variables like temperature, time, solvent concentration, and particle size. However, in our work the range of temperature studied is larger, including superheated water conditions, and our results are supported by the use of a novel semicontinuous reaction system that can yield more accurate and reliable measurements, as they are obtained as the result of the operation of the facility with comparatively larger quantities of reagents over a prolonged time, and not by sampling at a certain single time, as it has to be done with smaller batch systems. Therefore, the present study presents for the first time a potential integration of solvents-based CO_2 capture with green hydrogen generation at the same time. Coupling these two processes is of high relevance, specially to CO_2 emitting industries, who could benefit from using the generated hydrogen for self-consumption, or for offering the product in the hydrogen growing market. To demonstrate it, a novel semicontinuous facility was designed and constructed, giving important information for a future scaled-up process. This approach allowed determining the most active metallic-beds, and the catalyzing effect of using a CO_2-Rich stream (CO2RS) and a CO_2 Capture-Solvent Lean stream (CO2LS) in the green hydrogen generation.

Materials and methods

Chemicals

As CO_2-Rich streams (CO2RSs), ammonium carbamate (AC) (99%, Sigma Aldrich) and sodium bicarbonate (SB) (100%, COFARCAS-Spain) diluted in water MilliQ were used in concentrations of 0–3.0 mol/L. As CO_2 Capture-Solvent Lean streams (CO2LSs), aqueous solutions of ammonia (Panreac) (0.35–5 mol/L), ethanolamine (MEA) (Sigma Aldrich) (5 mol/L) or sodium hydroxide (NaOH) (Sigma Aldrich) (0.5 M) were used. The metallic-beds (MBs) used were: i) fine powder of Zn, ii) powder of Mn (≥99% trace metals basis), and iii) fine powder of Fe (≥99%), purchased from Sigma-Aldrich, iv) powder of Al (99.5%) purchased from Panreac, v) granular aluminum (<1 mm, 99.7% trace metals basis, Sigma-Aldrich), all considered PRMs, and as residue: vi) aluminum chips (provided by BEFESA company). Granular aluminum and Al chips were sieved into 250 and 500 μm sizes (mesh 60 and 35, respectively), and further employed without any other treatment.

Liquid and gas characterization

The ammonium carbamate liquid samples were analyzed by HPLC (Waters, Alliance separation module e2695) using an RAZEX™ ROA-Organic Acid H+ column with RI detector (Waters, 2414 module). The mobile phase was 25 mM H_2SO_4 with a flow rate of 0.5 mL/min. The temperatures of the column and the detector were 40 °C and 30 °C, respectively.

The hydrogen composition was quantified using a Micro-GC-TCD Varian 4900, equipped with Molsieve 5A-10 m and Poraplot Q –10 m columns. Two reference gas standard mixtures of H_2 at two different concentrations (5.0086 mol% H_2 and 94.9914 mol% CH_4; 50.0322 mol% H_2 49.9678 mol% CH_4), provided by BAM institute from Germany, were employed.

Design and operation of the semi-continuous H_2-generation facility

Fig. 1 shows the process flow diagram (PFD) of the designed system, where the main operation circuit is defined by the flow path of either CO2RS or CO2LS, starting in tank T-101, then the pump P-101 (HPLC pump Jasco), heater H-101, fixed bed reactor R-101, cooler C-101 (using ethylene glycol as refrigerant) and finally the flash drum S-101 (316 L Stainless Steel Double Ended DOT-Compliant Sample Cylinder-Swagelok) (see blue line in Fig. 1). Before each experiment, the circuit is dried out of any remaining water/moisture from a previous run, by flowing compressed air (opening V-01 and V-02), followed by leak testing with nitrogen (valve V-02) at 1.0 MPa above the vapor pressure of water at the corresponding experiment operation temperature (e.g., for 250 °C the leak testing pressure is 5.0 MPa: 4.0 MPa [vapor pressure] + 1.0 MPa). To reach and control the desired pressure, a back-pressure regulator (BPR) was installed before the three-way valve V-04. In a typical experience, the CO2RS or CO2LS are pumped through the circuit afore described, and the three-phase fixed bed reactor (ID 0.9525 cm, Length 10 cm with packed with 2 g of MB) is operated in co-current upflow mode, so the generated hydrogen follows the liquid motion, in likeness to the packed-bed bubble flow described by Dudukovic [62], while the reaction between water and the metals proceed in a semi-continuous fashion. Upstream the reactor, the two fluid phases (liquid and gas) are collected and split in liquid-gas separator S-101. The operational temperature of the facility ranges from room temperature up to conditions of superheated water (250 °C and 5.0 MPa), reaction time from 0.5 to 3 h of steady temperature time (STT), where time zero starts when reaching the working temperature, after a heating ramp of 30 °C/min. During the STT, valves

V-05 and V-06 remain closed, so S-101 is gradually filled with liquid and gas, making the internal pressure to increase proportionally to the volumetric flow of liquid and gas collected. Temperatures T1 and T2 were measured by K-type thermocouples (RS Components Ltd., accuracy: ±1.5 °C), and recorded by means of a Temperature Picotech instrument USB TC-08. T3 (Flash drum) was measured with a Pt-100 sensor (RS Components Ltd., accuracy: ±0.15 °C). Pressure P3 was measured by a digital Druck pressure gauge (model DPI-104-IS, accuracy of 0.05% FS). The experiments were duplicated to stablish the experimental uncertainty.

The moles of hydrogen produced (nH_2), at the end of STT, are calculated with equation (8) (Ideal Gas) and equation (9):

$$nH_{2=}\frac{P_{s,f} * V_{s,f}}{R^* T_{s,f}} * xH2 \quad (8)$$

$$V_{s,f} = V_{s,t} - V_{s,l} \quad (9)$$

Given the low pressure (<0.375 MPa) and temperature (room) of the hydrogen-containing gas inside the unit S-101, its behavior can be considered as ideal gas [63], and the application of the equation of ideal gases is adequate, so is not necessary to use a more complex equation. The fractional molar composition of hydrogen ($xH2$) was measured by MicroGC-TCD.

The response variables $Y\ H_2$ and $\varphi H2$ are calculated by equations (10)–(14):

$$n_{RM,MB} = \frac{W_{MB}}{MW_M} * X_{RM} \quad (10)$$

$$n_{H2,MB} = n_{RM,MB} * R_{H2,RM} \quad (11)$$

$$YH_{2=}\frac{nH_2}{n_{H2,MB}} * 100 \quad (12)$$

$$nH2_{STP} = \frac{Vs, f_{STP}}{Vn_{STP}} * xH2 \quad (13)$$

$$\varphi H_{2=}\frac{nH2_{STP}}{STT} * 100 \quad (14)$$

In the case of Al chips as MB the mass composition (wt%) of RMs (X_{RM}) was determined by XRF, and for PRMs (commercial powders of Al, Zn, Mn and Fe) was approximated to 100%. The molar volume of hydrogen at STP (Vn_{STP}) is 22.428 L/mol, according to NIST [64].

The CO_2 conversion (ICO2) is calculated by equation (15):

$$ICO2 = abs\left(\frac{C_{cs,f} - C_{cs,i}}{Ccs,\ i}\right) * 100 \quad (15)$$

Solid characterization

The solid samples were dried overnight in a vacuum-oven at 45 °C, to remove the remaining moisture. They were analyzed by X-ray diffraction (XRD), using a BRUKER D8 DISCOVER A25 equipment, with 3 kW Generator, 2.2 kW type FFF Cu-ceramic tube, LynxEye Detector, operating at 40 kV and 30 mA. The database used for identifying the phases was the PDF-2 Released 2013 (ICDD). SEM micrographs observations were conducted over raw Al 500 μm and Al chips to determine its morphology. For this, a Quanta 200FEG ESEM (Environmental Scanning Electron Microscope) equipment was used, operating at 20 kV. The samples were coated with gold in a K575

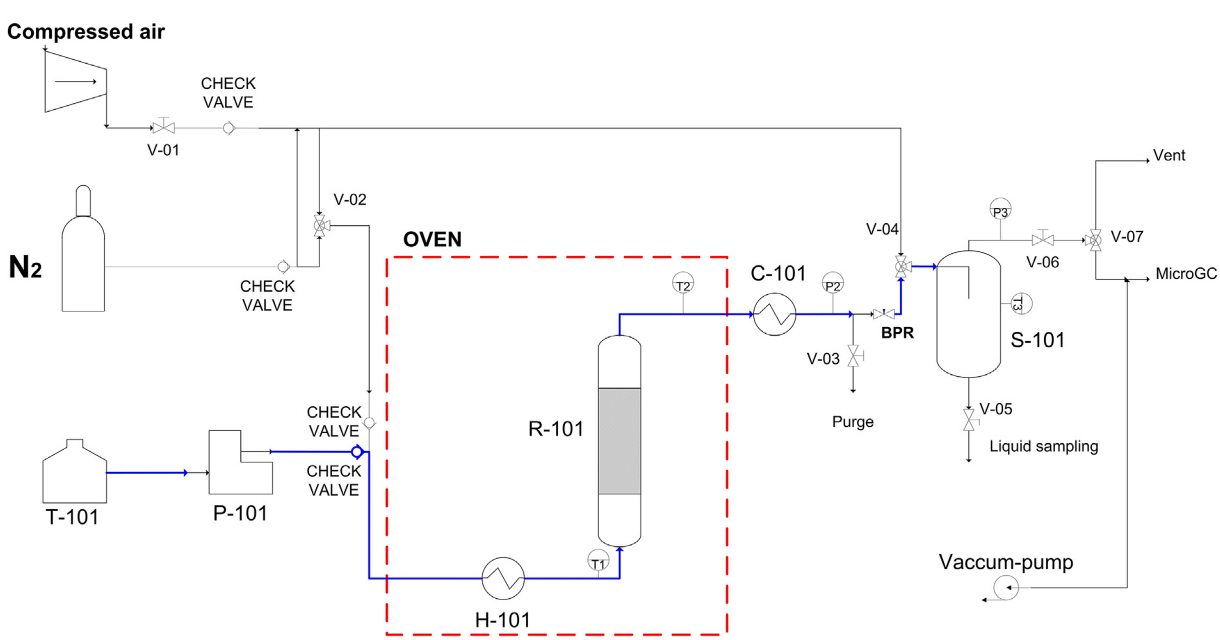

Fig. 1 – Process flow diagram of the semicontinuous hydrogen generation facility. T-101: solution tank, P-101: solution pump, H-101: solution heater, R-101: Fixed metallic-bed reactor, C-101: reactor's outlet cooler, BPR: Back pressure regulator, S-101: flash drum for liquid-gas separation. Blue line: main operation circuit. (For interpretation of the references to color in this figure legend, the reader is referred to the Web version of this article.)

sputter coater, and the images generated with a BSED detector. Textural properties analysis of the solids were conducted in an ASAP 2420 equipment with nitrogen adsorption at 77 K, all samples were degassed prior to each analysis. The surface area was determined by the BET method, while pore size and volume were calculated by the BJH method.

X-ray fluorescence (XRF) was employed to semi-quantitative determine the elementary composition of Al chips by means of a Bruker S8 TIGER spectrometer, equipped with a Rhodium tube anode and 4 KW excitation power, using LIF200, LIF220, PET Y XS-55 as analyzer crystals. Mean particle sizes (D90 percentile) of Al, Zn, Mn and Fe powders were measured by laser diffraction (Malvern Mastersizer 2000), using dry disperser accessory (Scirocco 2000).

Results and discussion

Performance of PRMs as MB on the hydrogen yield under aqueous ammonium carbamate as CO2RS

The hydrogen yield with respect to the PRMs was tested at the condition of superheated water (200 °C, 2.5 MPa) and 2 h of STT, using 1.5 mol/L of ammonium carbamate as CO2RS. Because ammonium carbamate flow rate did not affect the yield (see Fig. 1S), it was decided to fix this variable to 0.5 mL/min. From Fig. 2 it can be observed that the H_2 yield increased in the order Al < Mn < Fe < Zn, with a maximum H_2 yield of 75.3% for Zn, followed by Fe with 34%. Al and Mn showed marginal yields between 6 and 8%. The results for Zn and Fe powder are outstanding because it means they responded well to the proposed activation method without further modification or pretreatment (e.g., costly alloy preparation or doping process). Also, Zinc showed the highest activity toward hydrogen generation, even with the weak-base aqueous ammonium carbamate. Considering that particle size of Fe and Zn are comparable (19.61 ± 2.06 μm and 12.95 ± 0.19 μm, respectively), and that they displayed significatively different H_2 yield (76% and 26.5%, respectively), this suggest other factor, inherent to the metal, affecting the hydrogen generation performance, as will be discussed later on the light of the standard reduction potential. Similarly to the aim of the present work of utilizing CO_2 in basic solutions as activator of hydrogen generation, Xi et al. [55] studied the promoting effect that has the addition of ammonium salts like CH_3COONH_4 (among others) to Mn, owing to its anions' (CH_3COO^-) capacity to coagulate of $Mn(OH)_2$ passive layer, that prohibits the reaction to proceed. Likewise, Michiels et al. [56] also demonstrated the benefit of CO_2 in the oxidation of Iron to generate hydrogen and magnetite, by the formation of unstable intermediate iron (II) carbonate $FeCO_3$ that promotes the overall reaction.

In the present work, the hydrogen produced had associated a carbamate conversion (ICO2), detected by HLPC for all metals. The ICO2 had a maximum of 7.7% when using Mn, indicating that the CO_3^- anion has been either chemisorbed (recaptured) into the MB or decomposed to the gas phase, as will be discussed later in more detail with the solid characterization.

Comparison of pure Al and Al chips on hydrogen yield under aqueous ammonium carbamate as CO2RS

Based on the high economic potential that aluminum could have, given its abundance, lower price ($2.34/kg) compared to zinc ($2.89/kg) [65], and higher recyclability than other metals, pure Al and residual Al chips were selected for further evaluations. Both materials were sieved to 250 and 500 μm (mesh 60 and 35, respectively). Fig. 3 depicts them morphology, determined by SEM micrographs, where pure Al 500 μm present a regular and round shape morphology, while Al chips in contrast presented a distribution of irregular geometries, mostly with a curly sharp-shape, which difficult the sieving and handling.

To stablish the effect of textural properties of Al and Al chips, hydrogen generation experiments were conducted at conditions: 200 °C, 2.5 MPa, 2 h of STT and 0.5 mL/min of 1.5 mol/L of ammonium carbamate as CO2RS (see Table 1). As expected, a proportionality between the H_2-yield and the particle size for both aluminum types were found, where yield increased up to 9.2% for Al chips at 250 μm. This type of Al-residue showed better yield performance, in comparison to the pure aluminum, probably because of its higher surface area (4.68 m^2/g against 0.17 m^2/g for Al 250 μm), pore volume (6.05E-03 cm^3/g against 2.54E-04 cm^3/g) (see Table 1) and because its chemical composition is not limited only to elemental Al (90.5%), but also includes other RMs determined by XRF, such as Zn (2.25%), Si (1.42%), Mn (0.12%), Fe (0.64%), among others (see Fig. 4).

The differences of RMs' reactivity with water are due to the different values of reduction potential, where the more negative the value, the greater the tendency of metal to be oxidized. The different values of electronegativity in metals also contribute to the differences in reactivity with water, where the lower the value, the greater the tendency to lose electrons (become oxidized) (see Fig. 4). Metals with low electronegativity and more negative reduction potential like lithium, sodium, potassium (among others) are active enough at ambient temperature to react with cold water, producing the corresponding metal hydroxide and hydrogen [70]. Then, the fraction (~1.7 wt%) of elements of more negative reduction potential in Al-chips, such as Ca, K, Mg and Na, can either play a doping role or form alloys with aluminum, which are known as effective compounds in producing H_2 from alkaline solutions [38]. This result makes the Al chips a very promising residue for hydrogen generation, which can be directly utilized without costly pretreatments.

Effect of temperature and concentration of CO2RS on hydrogen yield

The influence of temperature and concentration on the H_2 generation was studied from 25 to 250 °C (2.5–5.0 MPa) using Al 500 μm, a flow of 0.5 mL/min of the CO2RS (aqueous ammonium carbamate and sodium bicarbonate) in the concentration range of 0–3.0 mol/L, and 2 h of STT (Fig. 5). It is known that the increase of temperature results in a faster Al-water reaction and a higher flow rate of produced hydrogen [71]. Accordingly, a proportionality of H_2 yield to temperature

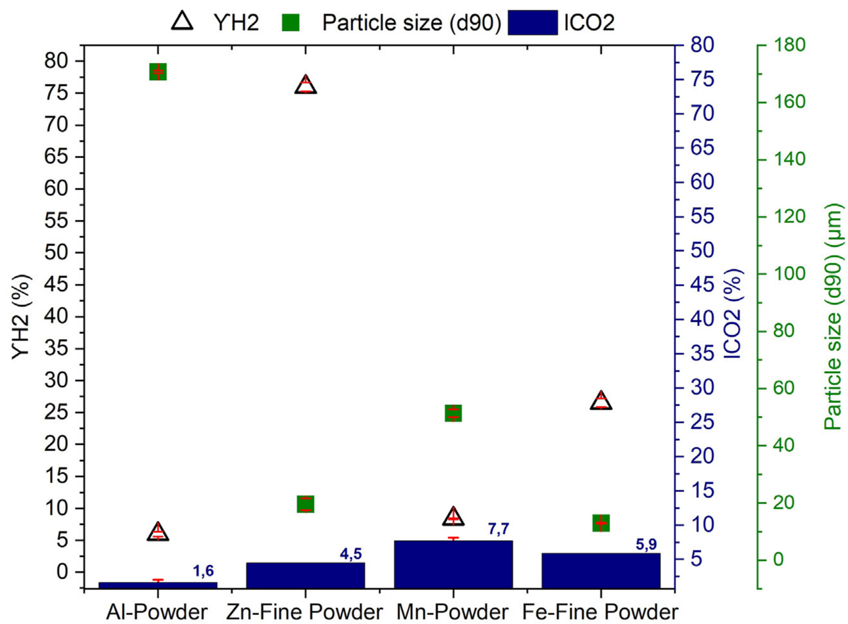

Fig. 2 – H_2 yield and CO_2 conversion (ICO2) as function of PRM type. Reaction conditions: 200 °C, 2.5 MPa, 2 h of STT and 0.5 mL/min of 1.5 mol/L of ammonium carbamate as CO2RS.

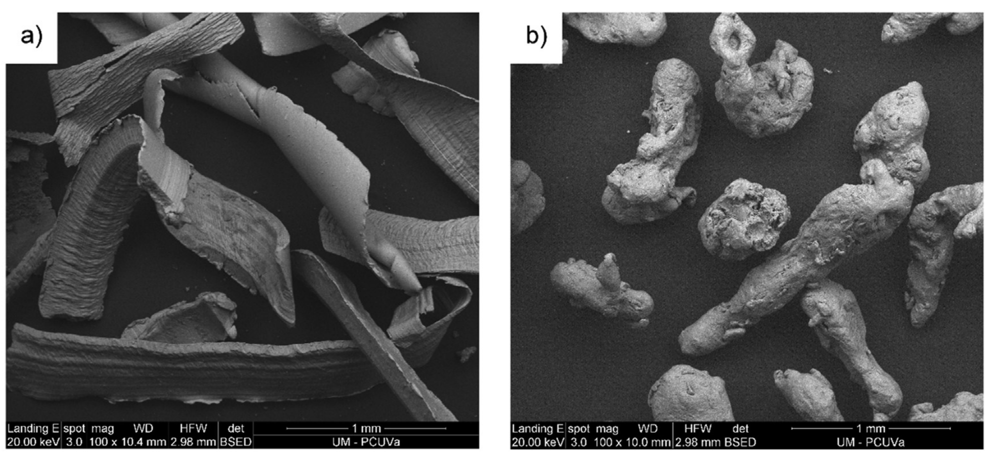

Fig. 3 – Morphology of a) Al chips 500 μm, and b) pure Al 500 μm.

was found with ammonium carbamate as activator, reaching its highest at 250 °C. Yield is also proportional to concentration of ammonium carbamate and starts to level off above at 1.5 mol/L, a trend that can be better observed at temperatures from 130 to 250 °C. For its part, sodium bicarbonate as activator contrasts radically with ammonium carbamate, as its performance is higher by far, reaching 71% and a hydrogen generation rate of 4.38 mmol/min, in only 0.5 h of STT and 1.0 mol/L concentration. Hydrogen generation is known to be faster at alkaline pH [72], and based on ion speciation studies of Ahn et al. [73], at temperature of 200 °C, carbamate solution significatively decreases the pH to 6.7 (slightly acidic) because of thermal decomposition of anion HCO_3^-, while sodium bicarbonate is not decomposed and conserve the alkalinity with pH = 8.8, evidencing the difference of yield results.

To stablish whether captured CO_2 in ammonia has a catalyzing role in the hydrogen generation, a reference experiment was performed with 0.35 mol/L of NH_3 at 200 °C, keeping the rest of reaction conditions unvaried. The H_2 yield was nearly the same as with 1.5 mol/L of ammonium carbamate and 200 °C, indicating that captured CO_2 in ammonia (mainly in the form of an equilibria of NH_2COO-, CO_3^- and HCO_3^- anions in aqueous solution [74]) does not have an appreciable catalyzing role in the aluminum water-splitting, considering two main reasons: i) carbamate is an amino-acid anion with a neutral character, ii) no carbonate intermediate is formed in the aluminum water-splitting, unlike carbonate-assisted hydrogen generation from iron, where CO_2 has a catalyzing role by the formation of the intermediate $FeCO_3$ compound that undergoes decomposition to Fe_3O_4 and CO_2 [56,75].

To have more insights about the feasibility of the different metallic bed tested, a simple cost analysis was conducted considering the available prices of the closest commercial

Table 1 – H_2 yield and cost as a function of MBs used. Reaction conditions: 200 °C, 2.5 MPa, 2 h of STT and 0.5 mL/min of 1.5 mol/L of ammonium carbamate as CO2RS.

Run	Metallic bed	Average Price ($/kg)	Particle size (μm)	Surface area (m^2/g)	Pore volume (cm^3/g)	Pore diameter (nm)	YH2 (%)	Cost of metallic bed per Kg of H_2 produced ($/kg)
1	Al powder	2.34[a]	170.7 ± 0.5[e]	0.12	7.12E-04	24.09	6.0 ± 0.4	350.7
2	Zn fine-powder	2.89[a]	19.6 ± 2.1[e]	0.24	4.54E-04	7.71	76.0 ± 0.7	124.3
3	Mn powder	2.26[b]	51.3 ± 1.3[e]	0.21	4.22E-04	8.26	8.4 ± 0.1	739.1
4	Fe fine-powder	0.51[c]	13.0 ± 0.2[e]	0.32	3.98E-04	4.98	26.5 ± 0.7	40.4
5	pure Al	2.34 [a]	250[f]	0.17	2.54E-04	6.07	2.2 ± 0.3	956.6
6	pure Al	2.34 [a]	500[f]	0.1	1.14E-04	4.71	1.6 ± 0.1	1315.3
7	Al chips	0.46[d]	250[f]	4.68	6.05E-03	5.18	9.2 ± 0.4	45.0
8	Al chips	0.46[d]	500[f]	1.17	2.17E-03	7.46	4.2 ± 0.4	98.5
9[g]	pure Al	2.34 [a]	500[f]	0.1	1.14E-04	4.71	85.5	24.6

[a] Aluminum and zinc from Ref. [65].
[b] Commercially found as electrolytic manganese metal from Ref. [66].
[c] Commercially found as direct reduced iron (DRI) (or sponge iron) from Ref. [67].
[d] Commercially found as aluminum turnings scrap from Ref. [68].
[e] d90 percentile (Mastersizer).
[f] Measured by sieving.
[g] Using NaOH 0.5 mol/L as CO2LS instead of ammonium carbamate as CO2RS.

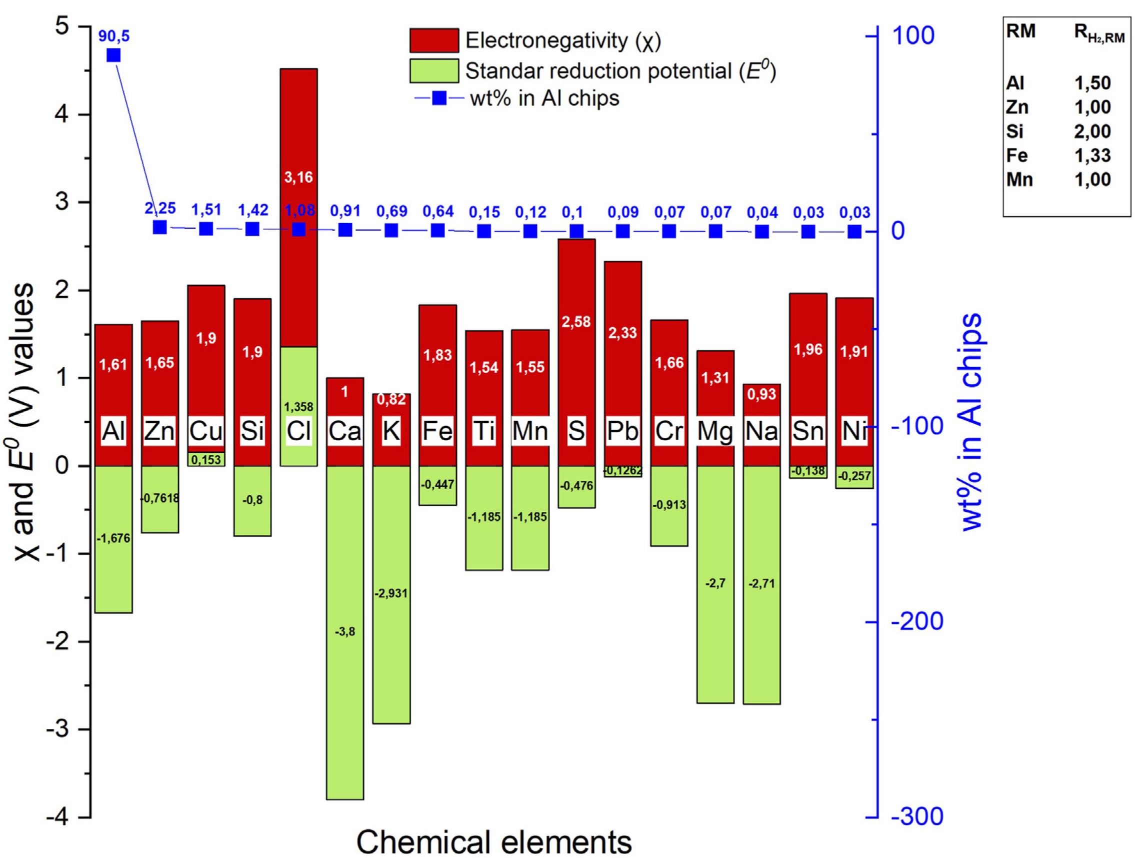

Fig. 4 – Elemental composition of Al chips (determined by XRF) and reduction potential and electronegativity values (taken from Ref. [69]).

commodities in the market (see Table 1). From the analysis, is clear that using pure expensive metals like Zn and Mn is not practical (although the study demonstrates the technical feasibility of using these metals, if they are available in lower cost metal residues), while cheaper and more abundant materials like aluminum, aluminum residues and Fe are closer to a techno-economic feasibility (cost of metallic bed as low as $40–45/kg_$H_2$). Besides, the cost impact of the metallic bed can be lowered by increasing the hydrogen yield through the activation with a more basic solvent like NaOH as

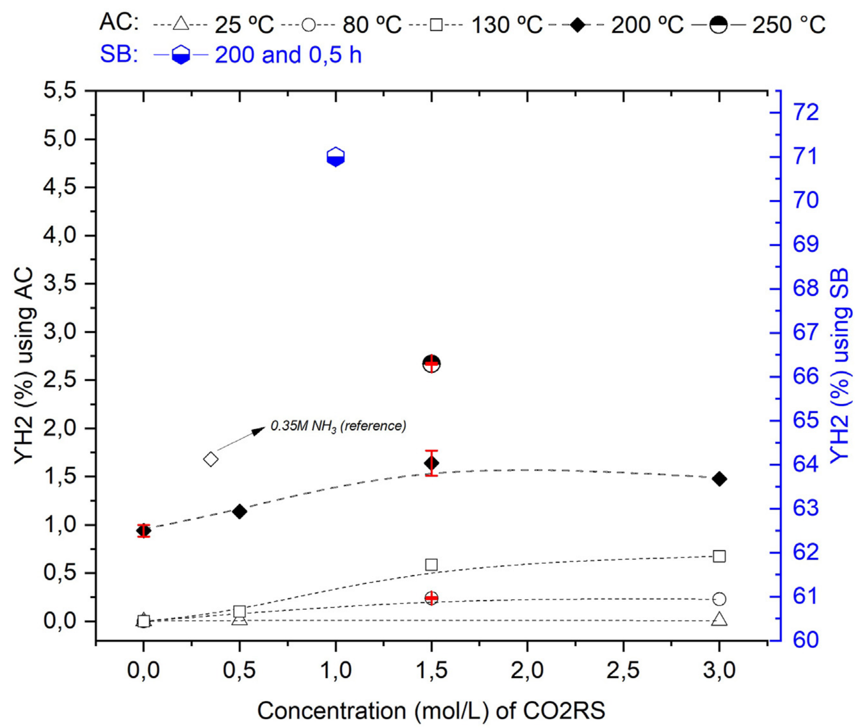

Fig. 5 – H_2 yield as function of temperature and concentration of ammonium carbamate. Reaction conditions: Al 500 μm, 25–250 °C (2.5–5.0 MPa), 0.5 mL/min of the CO2RS (ammonium carbamate and sodium bicarbonate), 0–3.0 mol/L, 2 h of STT.

observed with run 9, with cost of metallic bed as low as $24.6/kg_H2. Although requiring further optimization, this emerging technology has prospects, provided that the cost can be lowered to the order of magnitude of others, like photolysis and electrolysis with electricity from renewable sources (~$10/kg_H2) [31].

Green-hydrogen generation using CO2LSs

Fig. 6 depicts the hydrogen yield with respect to type and concentration of CO2LS (aqueous solutions of NH_3, NaOH and MEA) using pure Al 500 μm, at the conditions of superheated water (200 °C and 2.5 MPa), during 2 h of STT and 0.5 mL/min. If driven with solar/wind power, this hydrogen could be considered as green, as no CO_2 emissions are involved. It is remarkable that among the solvents used, NaOH enabled the highest H_2 yield (up to 85.5%), within only 50 min, at a low concentration of 0.5 mol/L. This experiment accounts for a hydrogen rate of 1.88 mmol/min, while a lesser rate of 0.44 mmol/min (at STP) was obtained in experiments of 25 °C and atmospheric pressure, but under much higher flow of 10 mL/min of KOH 0.5 M [54], and a rate of 0.33 mmol/min for 10 mL/min of 0.5 M NaOH [76]. These results fit well with what is stated in the field of sodium hydroxide for clean hydrogen production, because as compared to other activation methods, NaOH provides the higher rate of hydrogen generation [77]. In the case of NH_3, the H_2 yield reached a maximum of 2% at a concentration of 1.5 mol/L, and leveled off up to 5.0 mol/L, and with MEA the yield was marginal of 1.6% also at 5.0 mol/L. The disadvantage of using NaOH as an activator is its corrosive nature, but it is cheaper ($0.97/kg) than ammonia ($1.03/kg) [78] and MEA ($1.15/kg) [79]. However, through the present work, it is proposed to potential stakeholders (thermal power stations, ironmaking factories, concrete and cement factories, among others) to overcome this cost disadvantage utilizing the lean stream from the NaOH–CO_2 capture system before the absorption step, thus adding value by generating green hydrogen at the same time, while minimizing the CO_2 conversion of the CO2LSs by the high-pressure of the superheated-water condition. The increase of pressure can also improve the removal of CO_2 in the subsequent absorption column [80].

Given the outstanding performance of 0.5 mol/L NaOH, it was desired to conduct its evaluation at a much lower temperature of 25 °C, which is a mild temperature for capturing CO_2 in NaOH, while comparing it with ammonium carbamate under the same conditions. In Fig. 7, the H2 yield for NaOH in 3 h was 45.4%, while for ammonium carbamate it was less than 0.1% (the experiment was stopped at 2 h due to the evidence of no hydrogen generation). Interestingly, when registering the temperature in the outlet of the tubular reactor (T2 in Fig. 1), which corresponds to a point near the metal-bed, the behavior for NaOH showed temperature peaks pattern throughout the reaction time, observing three main peaks (about 28 °C) at 88.7, 136 and 183.5 min, while for ammonium carbamate the T2 behavior was flat, without these peaks. Likewise, when data-logging the pressure in the flash drum (P3 in Fig. 1), for NaOH peaks could also be observed that matched well with the temperature peaks, indicating that the hydrogen generation reaction is exothermic, exhibiting a pulses pattern, and demonstrating that, under the studied conditions, it can proceed in a self-sustaining way without

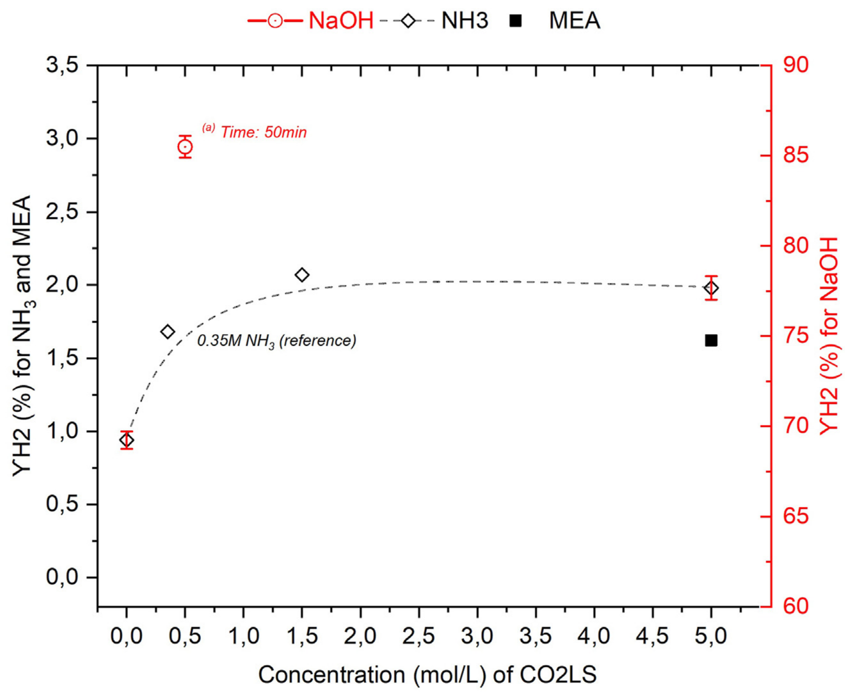

Fig. 6 – H_2 yield as function of concentration of different CO2LSs. Reaction conditions: Al 500 μm, 200 °C (2.5 MPa), 0.5 mL/min and 2 h of STT.

external energy input at ambient temperature. Hence, a recovery of heat is possible, considering an average enthalpy of aluminum-water splitting reaction at 25 °C of −846.5 kJ/mol [81]. For ammonium carbamate the increase of pressure is due to the continuous pumping of liquid and the subsequent filling-up of the flash drum that compresses the gas headspace.

Solid byproducts characterization

Characterization of byproducts of PRMs activation with aqueous ammonium carbamate stream as CO2RS

Fig. 8 depicts the XRD diffractograms of the solid byproduct from the experiments with selected PRMs that were analyzed in Fig. 2. For the case of Al, Fig. 8 a) shows the typical signals of

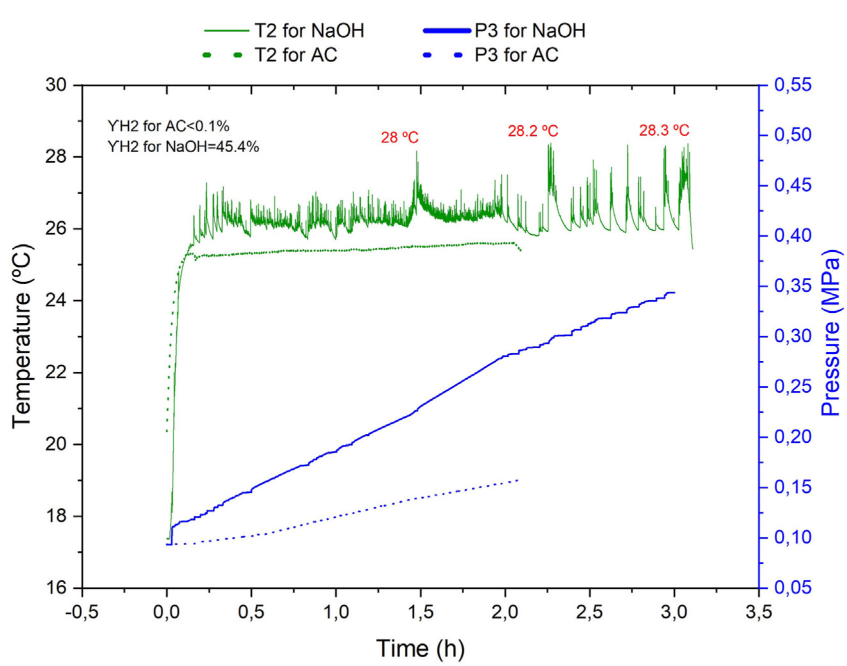

Fig. 7 – Temperature T2 and pressure P3 behavior during the activation of Al with aqueous ammonium carbamate and NaOH streams. Reaction conditions: Al 500 μm, 25 °C, atmospheric pressure, 0.5 mol/L, and 2–3 h of STT.

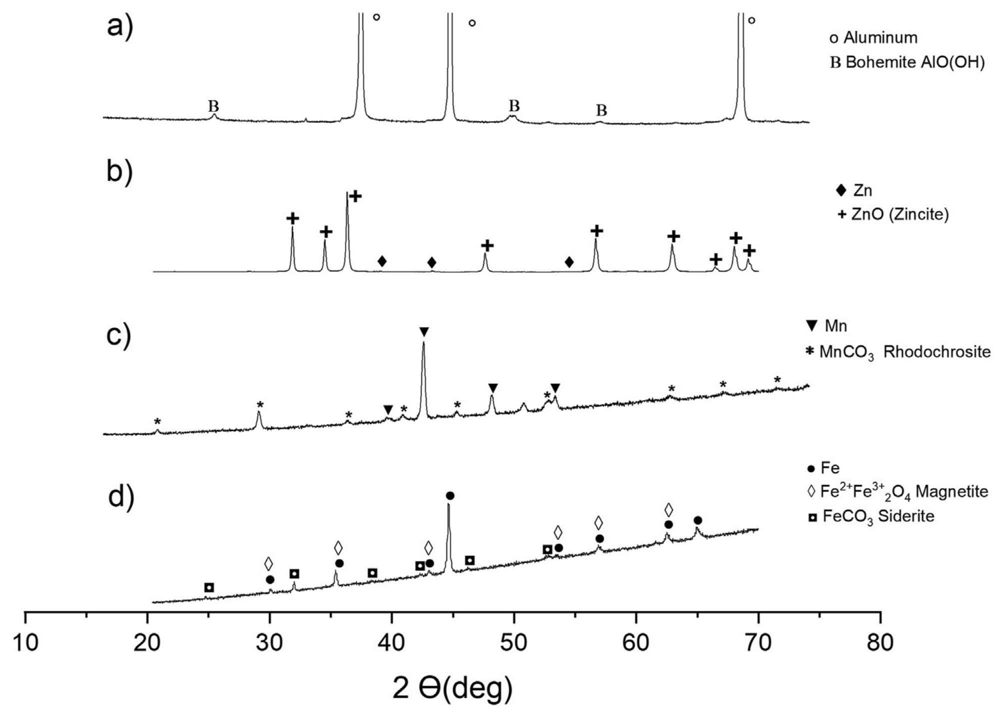

Fig. 8 – XRD diffractograms of solid byproducts after hydrogen generation with a) Al, b) Zn, c) Mn and d) Fe, using aqueous ammonium carbamate as CO2RS.

the cubic structure of elemental aluminum, with diffraction peaks at 2θ = 38, 45 and 65° [82,83] (PDF 00-004-0787) confirming that is only partially exhausted into boehmite (2θ = 28, 49 and 55°) (PDF 00-021-1307) [84] to generate hydrogen. Diffractogram of Fig. 8 b) confirms the almost complete exhausting of Zn (weak peaks at 39, 43.3 and 54.3°) (PDF 00-004-0831) into ZnO (31.8, 34.2, 36.2, 47.5, 56.6, 62.9, 66.2, 68 and 69°) [85] (PDF 00-036-1451) for the highest H2 yield of 75% (Fig. 2). Diffractogram of

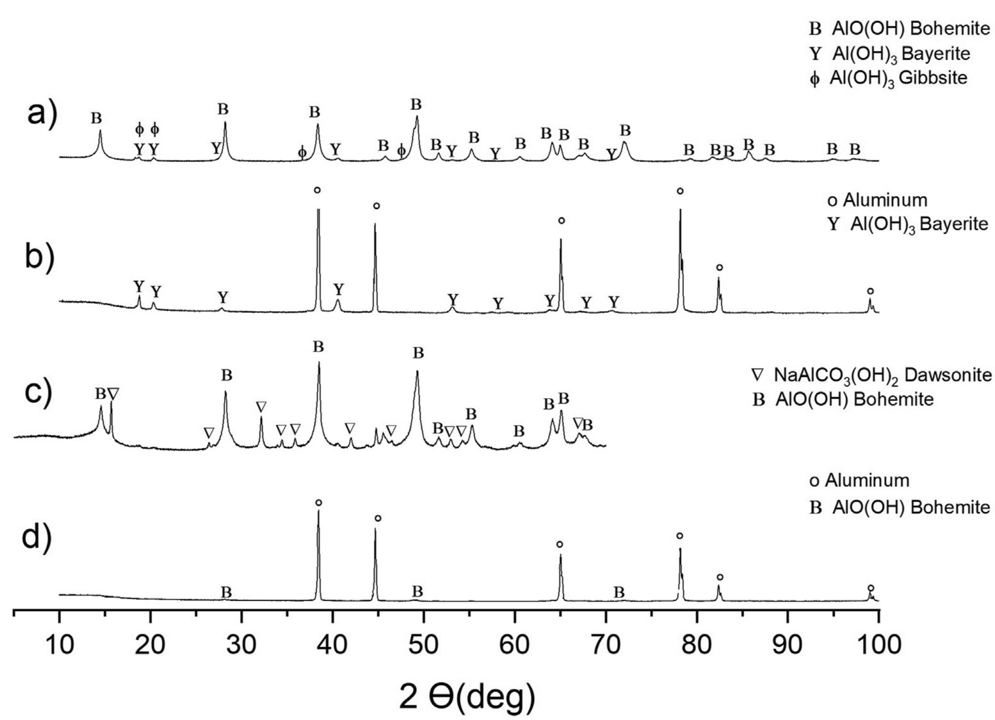

Fig. 9 – XRD diffractograms of solid byproduct after activation of pure Al 500 μm with a) NaOH at 200 °C and 0.8 h, b) NaOH at 25 °C and 3 h, c) sodium bicarbonate at 200 °C and 0.5 h, and d) ammonium carbamate at 200 °C and 2 h.

Fig. 8 c) suggest that the capture CO2 of the CO2RS was chemisorbed by Mn (40.5, 42.9, 47.7 and 52.3) to form MnCO3 Rhodochrosite (24.1, 31.2, 37.6, 41.3, 45.1, 51.5, 60, 63.9, 67.8°) [86] (PDF 00-044-1472). Diffractogram of Fig. 8 d) also suggests that the CO2 captured in the CO2RS was chemisorbed by Fe (30, 35.5, 43, 44.7, 53.5, 57, 62.6 and 65°) (PDF 00-006-0696) to form the hydrogen-promoting intermediate FeCO3 Siderite [56] (PDF 00-029-0696) [87], and the oxidation product Fe2+Fe3+2O4 Magnetite (PDF 00-019-0629) were also detected.

Characterization of byproducts of pure-aluminum activation with aqueous NaOH and $NaHCO_3$ (sodium bicarbonate) as CO2LS

Based on the diffractogram presented on Fig. 9 (a), the full conversion of aluminum by NaOH 0.5 M at 200 °C and 0.8 h for a H2 yield of 85.5% (Fig. 6) is confirmed, as the three possible oxidation products appeared, namely Bohemite AlO(OH) (PDF 01-083-2384), Bayerite Al(OH)3 (PDF 00-020-0011) and Gibbsite Al(OH)3 (PDF 00-007-0324). The water splitting reaction of aluminum with the aid of sodium hydroxide is written as in reaction (2), where 2 mol of sodium aluminate NaAl(OH)4 are formed. However, this compound was not detected by the XRD, therefore it could have been completely transformed to NaOH and Al(OH)3, according to reaction (16), thanks to the high conversion degree of the overall process [88]:

$$NaAl(OH)_4 \rightarrow NaOH + Al(OH)_3 \tag{16}$$

The diffractogram of byproducts after activation with NaOH 0.5 M at 25 °C and 3 h (Fig. 9. (b)) confirms its efficacy even at low temperature (H2 yield of 45.4%), while the proportion of bayerite peaks are lower to the elemental aluminum. The diffractogram of sodium bicarbonate byproduct at 200° and 0.5 h (Fig. 9. (c)) is consistent with the high oxidation degree of aluminum (H2 yield of 71%), in which elemental aluminum signals are faded out by boehmite and NaAlCO3(OH)2 Dawsonite signals (PDF 00-045-1359). In the same way, the diffractogram of ammonium carbamate byproduct at 200° and 2 h (Fig. 9. (d)) is consistent with the low oxidation degree of aluminum (H2 yield of 1.6%), in which elemental aluminum signal is the predominant, only accompanied by weak peaks of Bohemite.

Conclusions

For the first time, the coupling of CO2-Rich stream (CO2RS) and CO2 Capture-Solvent Lean stream (CO2LS) with the metals-based hydrothermal generation of hydrogen was successfully accomplished via the design of a novel semi-continuous facility. H_2 yield increased with both temperature and concentration of ammonium carbamate, while the flow of aqueous stream showed no significant effect. Remarkably, aqueous sodium bicarbonate (CO2RS) showed a greater performance in comparison to ammonium carbamate, by reaching 71% of H_2 yield, using Al, in only 0.5 h of STT at 200 °C and 1.0 mol/L concentration. Likewise, aqueous NaOH 0.5 mol/L (CO2LS) showed the highest H_2 yield (up to 85.5%), using Al, within only 50 min. This suggests that the most basic CO2RSs and CO2LSs like aqueous sodium bicarbonate and NaOH, respectively, can convert the most with less active or large size metallic beds, like Al and Mn tested in the present work. More active or small size beds do not require strong bases. From a simple cost analysis, it was concluded that using pure expensive metals like Zn and Mn is not practical, while cheaper and more abundant materials like aluminum, aluminum residues and iron are closer to a techno-economic feasibility, while the cost impact of the metallic bed can be lowered by the activation with a more basic solvent like NaOH. In the future, potential stakeholders that can assume the proposed technology of this paper are those enterprises applying solvents-based CO_2 capture systems in them productive processes: e.g., thermal power stations, ironmaking factories, concrete, and cement factories, among others. This may represent an opportunity for bringing about value-added to them economic activity, by generating at the same time a demand-growing item, like green hydrogen. The semi-continuous process presented in the present work set a precedent for further economic assessments, in search for the implementation of this new technology.

Declaration of competing interest

The authors declare that they have no known competing financial interests or personal relationships that could have appeared to influence the work reported in this paper.

Acknowledgements

This project has been funded by the Ministry of Science and Universities through project RTI2018-097456-B-I00 and by the Junta de Castilla y León through project by FEDER FUNDS under the BioEcoUVa Strategic Program (CLU-2019-04). Juan Ignacio del Río acknowledges Universidad de Valladolid for the predoctoral and postdoctoral fellowships, as well as to the company BEFESA for providing the Al-chips residue for the research.

Appendix A. Supplementary data

Supplementary data to this article can be found online at https://doi.org/10.1016/j.ijhydene.2023.04.021.

REFERENCES

[1] Rubio-Varas M, Munoz Delgado B. 200 years diversifying the energy mix? Diversification paths of the energy baskets of European early comers vs. latecomers. 2017.
[2] Center BP. Annual energy outlook 2020. Energy inf adm Washington, DC12; 2020. p. 1672–9.
[3] Iea R. Energy technology perspectives 2020. Spec rep carbon capture, util storage. 2020.

[4] Yu H, Qi G, Wang S, Morgan S, Allport A, Cottrell A, et al. Results from trialling aqueous ammonia-based post-combustion capture in a pilot plant at Munmorah Power Station: gas purity and solid precipitation in the stripper. Int J Greenh Gas Control 2012;10:15–25.
[5] Nocito F, Dibenedetto A. Atmospheric CO2 mitigation technologies: carbon capture utilization and storage. Curr Opin Green Sustain Chem 2020;21:34–43. https://doi.org/10.1016/j.cogsc.2019.10.002.
[6] Borhani TN, Wang M. Role of solvents in CO2 capture processes: the review of selection and design methods. Renew Sustain Energy Rev 2019;114:109299.
[7] Borhani TNG, Azarpour A, Akbari V, Wan Alwi SR, Manan ZA. CO2 capture with potassium carbonate solutions: a state-of-the-art review. Int J Greenh Gas Control 2015;41:142–62. https://doi.org/10.1016/j.ijggc.2015.06.026.
[8] Plaza MG, Martinez S, Rubiera F. CO2 capture, use, and storage in the cement industry: state of the art and expectations. Energies 2020;13:5692.
[9] Saravanan A, Vo D-VN, Jeevanantham S, Bhuvaneswari V, Narayanan VA, Yaashikaa PR, et al. A comprehensive review on different approaches for CO2 utilization and conversion pathways. Chem Eng Sci 2021;236:116515.
[10] Abe JO, Popoola API, Ajenifuja E, Popoola OM. Hydrogen energy, economy and storage: review and recommendation. Int J Hydrogen Energy 2019;44:15072–86.
[11] van Renssen S. The hydrogen solution? Nat Clim Change 2020;10:799–801.
[12] Commission ECE. Europe's moment: repair and prepare for the next generation. Commun from Comm 2020;456. https://www.eumonitor.eu/9353000/1/j9vvik7m1c3gyxp/vl90q3gs1wu2.
[13] Mirowski T, Janusz P. Hydrogen in energy balance–selected issues. Zesz Nauk Inst Gospod Surowcami Miner Pol Akad Nauk 2018;102:51–64.
[14] Hordeski MF. Alternative fuels: the future of hydrogen. CRC Press; 2020.
[15] Nikolaidis P, Poullikkas A. A comparative overview of hydrogen production processes. Renew Sustain Energy Rev 2017;67:597–611.
[16] Liu S, Zhang C, Sun Y, Chen Q, He L, Zhang K, et al. Design of metal-organic framework-based photocatalysts for hydrogen generation. Coord Chem Rev 2020;413:213266.
[17] Chen L-F, Hou C-C, Zou L, Kitta M, Xu Q. Uniformly bimetal-decorated holey carbon nanorods derived from metal–organic framework for efficient hydrogen evolution. Sci Bull 2021;66:170–8.
[18] Zhou F, Zhou Y, Liu G-G, Wang C-T, Wang J. Recent advances in nanostructured electrocatalysts for hydrogen evolution reaction. Rare Met 2021;40:3375–405.
[19] Li C, Zhu D, Cheng S, Zuo Y, Wang Y, Ma C, et al. Recent research progress of bimetallic phosphides-based nanomaterials as cocatalyst for photocatalytic hydrogen evolution. Chin Chem Lett 2022;33:1141–53.
[20] Ball M, Wietschel M. The future of hydrogen – opportunities and challenges. Int J Hydrogen Energy 2009;34:615–27. https://doi.org/10.1016/j.ijhydene.2008.11.014.
[21] van der Spek M, Banet C, Bauer C, Gabrielli P, Goldthorpe W, Mazzotti M, et al. Perspective on the hydrogen economy as a pathway to reach net-zero CO 2 emissions in Europe. Energy Environ Sci 2022;15:1034–77.
[22] Ishaq H, Dincer I, Crawford C. A review on hydrogen production and utilization: challenges and opportunities. Int J Hydrogen Energy 2021;47:26238–64.
[23] Yu M, Wang K, Vredenburg H. Insights into low-carbon hydrogen production methods: green, blue and aqua hydrogen. Int J Hydrogen Energy 2021;46:21261–73.
[24] Meldahl LL. A clean hydrogen market in the making. Comparing Norway's and the Netherland's roles in the European hydrogen transition. NTNU; 2021.
[25] Philibert C. Perspectives on a hydrogen strategy for the European union. Ifri: Etudes l'Ifri; 2020.
[26] Howarth RW, Jacobson MZ. How green is blue hydrogen? Energy Sci Eng 2021;9:1676–87.
[27] Neff J, Bataille C, Shaffer B. The role of hydrogen in decarbonizing Alberta's electricity system. Sch Public Policy Publ; 2021.
[28] Hjeij D, Bicer Y, Koç M. Hydrogen strategy as an energy transition and economic transformation avenue for natural gas exporting countries: Qatar as a case study. Int J Hydrogen Energy 2021;47:4977–5008.
[29] Acar C, Dincer I. Review and evaluation of hydrogen production options for better environment. J Clean Prod 2019;218:835–49.
[30] Rashid MM, Al Mesfer MK, Naseem H, Danish M. Hydrogen production by water electrolysis: a review of alkaline water electrolysis, PEM water electrolysis and high temperature water electrolysis. Int J Eng Adv Technol 2015;4:2249–8958.
[31] Shiva Kumar S, Himabindu V. Hydrogen production by PEM water electrolysis – a review. Mater Sci Energy Technol 2019;2:442–54. https://doi.org/10.1016/j.mset.2019.03.002.
[32] Kayfeci M, Kecebas A, Bayat M. In: Calise F, D Accadia MD, Santarelli M, Lanzini A, Ferrero, editors. Chapter 3 - hydrogen production. Academic Press; 2019. p. 45–83. https://doi.org/10.1016/B978-0-12-814853-2.00003-5.
[33] Huang X, Gao T, Pan X, Wei D, Lv C, Qin L, et al. A review: feasibility of hydrogen generation from the reaction between aluminum and water for fuel cell applications. J Power Sources 2013;229:133–40.
[34] Kutz M. Environmentally conscious materials and chemicals processing, vol. 3. New Jersey: Wiley Online Library; 2007.
[35] Steinfeld A, Kuhn P, Reller A, Palumbo R, Murray J, Tamaura Y. Solar-processed metals as clean energy carriers and water-splitters. Int J Hydrogen Energy 1998;23:767–74.
[36] Cho YS, Kim JH. Hydrogen production by splitting water on solid acid materials by thermal dissociation. Int J Hydrogen Energy 2011;36:8192–202.
[37] Lee S, Na UJ, Jo H. Techno-economic assessment of green hydrogen production via two-step thermochemical water splitting using microwave. Int J Hydrogen Energy 2023;48:10706–23.
[38] Wang HZ, Leung DYC, Leung MKH, Ni M. A review on hydrogen production using aluminum and aluminum alloys. Renew Sustain Energy Rev 2009;13:845–53. https://doi.org/10.1016/j.rser.2008.02.009.
[39] Setiani P, Watanabe N, Sondari RR, Tsuchiya N. Mechanisms and kinetic model of hydrogen production in the hydrothermal treatment of waste aluminum. Mater Renew Sustain Energy 2018;7:10.
[40] Turn S, Kinoshita C, Zhang Z, Ishimura D, Zhou J. An experimental investigation of hydrogen production from biomass gasification. Int J Hydrogen Energy 1998;23:641–8.
[41] Watanabe M, Jiang X, Saito R. Method for generating hydrogen gas utilizing activated aluminum fine particles26; 2007. U.S. Patent No 7,235,226.
[42] Amberchan G, Lopez I, Ehlke B, Barnett J, Bao NY, Allen A, et al. Aluminum nanoparticles from a Ga–Al composite for water splitting and hydrogen generation. ACS Appl Nano Mater 2022;5:2636–43.

[43] Gai W-Z, Zhang X, Sun K, Deng Z-Y. Hydrogen generation from Al-Water reaction promoted by MB/γ-Al2O3 (M= Co, Ni) catalyst. Int J Hydrogen Energy 2019;44:24377–86.
[44] Razavi-Tousi SS, Szpunar JA. Effect of structural evolution of aluminum powder during ball milling on hydrogen generation in aluminum–water reaction. Int J Hydrogen Energy 2013;38:795–806.
[45] Yang Y, Gai W-Z, Deng Z-Y, Zhou J-G. Hydrogen generation by the reaction of Al with water promoted by an ultrasonically prepared Al (OH) 3 suspension. Int J Hydrogen Energy 2014;39:18734–42.
[46] Macanas J, Soler L, Candela AM, Munoz M, Casado J. Hydrogen generation by aluminum corrosion in aqueous alkaline solutions of inorganic promoters: the AlHidrox process. Energy 2011;36:2493–501.
[47] Tekade SP, Shende DZ, Wasewar KL. Hydrogen generation in water splitting reaction using aluminum: effect of NaOH concentration and reaction modelling using SCM. Int J Chem React Eng 2018;16.
[48] Troczynski T, Czech E. Compositions and methods for generating hydrogen from water. 2005. U.S. Patent Application No. 11/103,994.
[49] Aleksandrov YA, Tsyganova EI, Pisarev AL. Reaction of aluminum with dilute aqueous NaOH solutions. Russ J Gen Chem 2003;73.
[50] Irankhah A, Fattahi SMS, Salem M. Hydrogen generation using activated aluminum/water reaction. Int J Hydrogen Energy 2018;43:15739–48.
[51] Martinez SS, Benites WL, Gallegos AAA, Sebastian PJ. Recycling of aluminum to produce green energy. Sol Energy Mater Sol Cells 2005;88:237–43.
[52] Ma G-L, Dai H-B, Zhuang D-W, Xia H-J, Wang P. Controlled hydrogen generation by reaction of aluminum/sodium hydroxide/sodium stannate solid mixture with water. Int J Hydrogen Energy 2012;37:5811–6.
[53] Belitskus D. Reaction of aluminum with sodium hydroxide solution as a source of hydrogen. J Electrochem Soc 1970;117:1097.
[54] Tekade SP, Shende DZ, Wasewar KL. Hydrogen generation in an annular micro-reactor: an experimental investigation of water splitting reaction using aluminum in presence of potassium hydroxide. Int J Chem React Eng 2018;17.
[55] Xi X, Chang J, Huang Z. The study of kinetics and reaction between metallic manganese and water in (NH~ 4)~ 2SÕ 4 solution. J Funct Mater 2003;34:320–2.
[56] Michiels K, Spooren J, Meynen V. Production of hydrogen gas from water by the oxidation of metallic iron under mild hydrothermal conditions, assisted by in situ formed carbonate ions. Fuel 2015;160:205–16.
[57] Mao Y, Gao Y, Dong W, Wu H, Song Z, Zhao X, et al. af. Appl Energy 2020;267:114860.
[58] Shmelev V, Nikolaev V, Lee JH, Yim C. Hydrogen production by reaction of aluminum with water. Int J Hydrogen Energy 2016;41:16664–73.
[59] Hiraki T, Yamauchi S, Iida M, Uesugi H, Akiyama T. Process for recycling waste aluminum with generation of high-pressure hydrogen. Environ Sci Technol 2007;41:4454–7.
[60] Takahashi H, Kori T, Onoki T, Tohji K, Yamasaki N. Hydrothermal processing of metal based compounds and carbon dioxide for the synthesis of organic compounds. J Mater Sci 2008;43:2487–91.
[61] Roychowdhury S, Ali MM, Dhua S, Sundararajan T, Rao GR. Thermochemical hydrogen production using Rh/CeO2/γ-Al2O3 catalyst by steam reforming of ethanol and water splitting in a packed bed reactor. Int J Hydrogen Energy 2021;46:19254–69.
[62] Dudukovic MP, Larachi F, Mills PL. Multiphase reactors–revisited. Chem Eng Sci 1999;54:1975–95.
[63] Cengel YA, Boles MA, Kanoglu M. Thermodynamics: an engineering approach, vol. 5. New York: McGraw-hill; 2011.
[64] Lemmon EW. Thermophysical properties of fluid systems. Nat. Inst. Stand. Tech. Gaithersburg; 1998.
[65] BusinessInsider. Aluminum and zinc prices. 2023. https://markets.businessinsider.com/commodities. [Accessed 24 March 2023].
[66] SMM-Shanghai Metals Market. Electrolytic manganese metal price. https://www.metal.com/Manganese/201102250594. [Accessed 23 March 2023].
[67] Steelmint. Direct reduced iron price. 2023. https://www.steelmint.com/v2019/spongeiron-prices-global. [Accessed 24 March 2023].
[68] Recycleinme. Aluminum turnings price. 2023. https://www.recycleinme.com/scrapresources/DetailedPrice?psect=1&cat=Canada Scrap Prices&subcat=Aluminum Turnings. [Accessed 24 March 2023].
[69] Haynes WM, Lide DR, Bruno TJ. CRC handbook of chemistry and physics. CRC press; 2016.
[70] Xu S, Liu J. Metal-based direct hydrogen generation as unconventional high density energy. Front Energy 2019;13:27–53.
[71] Yavor Y, Goroshin S, Bergthorson JM, Frost DL, Stowe R, Ringuette S. Enhanced hydrogen generation from aluminum–water reactions. Int J Hydrogen Energy 2013;38:14992–5002.
[72] Soler L, Macanas J, Munoz M, Casado J. Synergistic hydrogen generation from aluminum, aluminum alloys and sodium borohydride in aqueous solutions. Int J Hydrogen Energy 2007;32:4702–10.
[73] Ahn CK, Lee HW, Chang YS, Han K, Kim JY, Rhee CH, et al. Characterization of ammonia-based CO2 capture process using ion speciation. Int J Greenh Gas Control 2011;5:1606–13.
[74] Ahn CK, Lee HW, Lee MW, Chang YS, Han K, Rhee CH, et al. Determination of ammonium salt/ion speciation in the CO2 absorption process using ammonia solution: modeling and experimental approaches. Energy Proc 2011;4:541–7. https://doi.org/10.1016/j.egypro.2011.01.086.
[75] Jin F, Gao Y, Jin Y, Zhang Y, Cao J, Wei Z, et al. High-yield reduction of carbon dioxide into formic acid by zero-valent metal/metal oxide redox cycles. Energy Environ Sci 2011;4:881–4. https://doi.org/10.1039/C0EE00661K.
[76] Tekade SP, Shende DZ, Wasewar KL. Hydrogen generation in an annular micro-reactor: an experimental investigation and reaction modelling by shrinking core model (SCM). Int J Chem React Eng 2018;16.
[77] Kumar S. Clean hydrogen production methods. Springer; 2015.
[78] Chemicals indexes. 2022. https://businessanalytiq.com/procurementanalytics/index/. [Accessed 22 November 2022].
[79] Elliott WR. FRONT-END engineering design (feed) study for a carbon capture plant retrofit to a natural gas-fired gas turbine combined cycle power plant appendixvol. 2. Reston, VA (United States): Bechtel National, Inc.; 2021.
[80] Qi G, Wang S, Yu H, Feron P, Chen C. Rate-based modeling of CO2 absorption in aqueous NH3 in a packed column. Energy Proc 2013;37:1968–76.
[81] Godart P, Fischman J, Seto K, Hart D. Hydrogen production from aluminum-water reactions subject to varied pressures and temperatures. Int J Hydrogen Energy 2019;44:11448–58.
[82] Ravichandran M, Naveen Sait A, Anandakrishnan V. Densification and deformation studies on powder metallurgy Al–TiO2–Gr composite during cold upsetting. J Mater Res 2014;29:1480–7. https://doi.org/10.1557/jmr.2014.143.
[83] Kwon H, Leparoux M. Hot extruded carbon nanotube reinforced aluminum matrix composite materials. Nanotechnology 2012;23:415701.

[84] Liu Y, Ma D, Han X, Bao X, Frandsen W, Wang D, et al. Hydrothermal synthesis of microscale boehmite and gamma nanoleaves alumina. Mater Lett 2008;62:1297–301.
[85] Xing L-L, Ma C-H, Chen Z-H, Chen Y-J, Xue X-Y. High gas sensing performance of one-step-synthesized Pd–ZnO nanoflowers due to surface reactions and modifications. Nanotechnology 2011;22:215501.
[86] Liang W, Li L, Li R, Yin Y, Li Z, Liu X, et al. Crystal structure of impurity-free rhodochrosite (MnCO3) and thermal expansion properties. Phys Chem Miner 2020;47:1–11.
[87] Roh Y, Zhang C-L, Vali H, Lauf RJ, Zhou J, Phelps TJ. Biogeochemical and environmental factors in Fe biomineralization: magnetite and siderite formation. Clay Clay Miner 2003;51:83–95.
[88] Soler L, Macanas J, Munoz M, Casado J. Hydrogen generation from aluminum in a non-consumable potassium hydroxide solution. Proc. Int. Hydrog. Energy Congr. Exhib. IHEC 2005:13–5.